Performance Analysis of SmallSat Aerocapture at Venus

Rafael Lugo[1], Soumyo Dutta[1]
NASA Langley Research Center, Hampton, Virginia 23681, USA

Daniel Matz[2], Breanna Johnson[3]
NASA Johnson Space Center, Houston, Texas 77058, USA

Alejandro Pensado[4], Evan Roelke[4], John Aguirre[5], and Richard Powell[6]
Analytical Mechanics Associates, Hampton, Virginia 23666, USA

Aerocapture is a method of spacecraft orbital insertion that has the potential to provide mass savings as compared to aerobraking. In particular, aerocapture at Venus is desirable due to high atmospheric density and potential for science return. While promising, accurate orbital insertion by means of aerocapture requires an active guidance, navigation, and control architecture. This paper documents the initial assessment of the performance of two guidance algorithms, a generalized numerical predictor corrector and the Fully-Numeric Predictor-corrector for Aerocapture Guidance, applied to smallsat aerocapture at Venus using two different simulation environments with equivalent simulation inputs. Nominal trajectory performance is assessed. In addition, Monte Carlo analysis is performed to compare each guidance algorithm's performance under uncertainty.

I. Introduction

Detailed studies of the planets and moons in our Solar System typically require an orbiting spacecraft or planetary probe equipped with science instrumentation that can provide and transmit relevant data about the planet, its atmosphere, and surface. A significant challenge to this approach is accurately inserting the spacecraft into its desired orbit about the planet. Various methods exist, including fully-propulsive orbit insertion, aerobraking, and aerocapture. Both fully-propulsive insertion and aerobraking utilize the thrust of the onboard engines to decelerate the vehicle and maneuver the spacecraft into its final orbit. Aerobraking takes advantage of the aerodynamic drag generated when the spacecraft skims the upper layers of the atmosphere and requires less propellent than fully-propulsive orbit insertion. However, aerobraking is time- and resource-intensive as it requires multiple monitored passes through the atmosphere before the final orbit is reached.

---

[1] Aerospace Engineer, Atmospheric Flight and Entry Systems Branch, AIAA Senior Member.
[2] Aerospace Engineer, Flight Mechanics and Trajectory Design Branch, AIAA Senior Member.
[3] Aerospace Engineer, Flight Mechanics and Trajectory Design Branch, AIAA Member
[4] Aerospace Engineer, Atmospheric Flight and Entry Systems Branch, AIAA Member.
[5] Computer Scientist, Atmospheric Flight and Entry Systems Branch.
[6] Aerospace Engineer, Atmospheric Flight and Entry Systems Branch, AIAA Fellow.

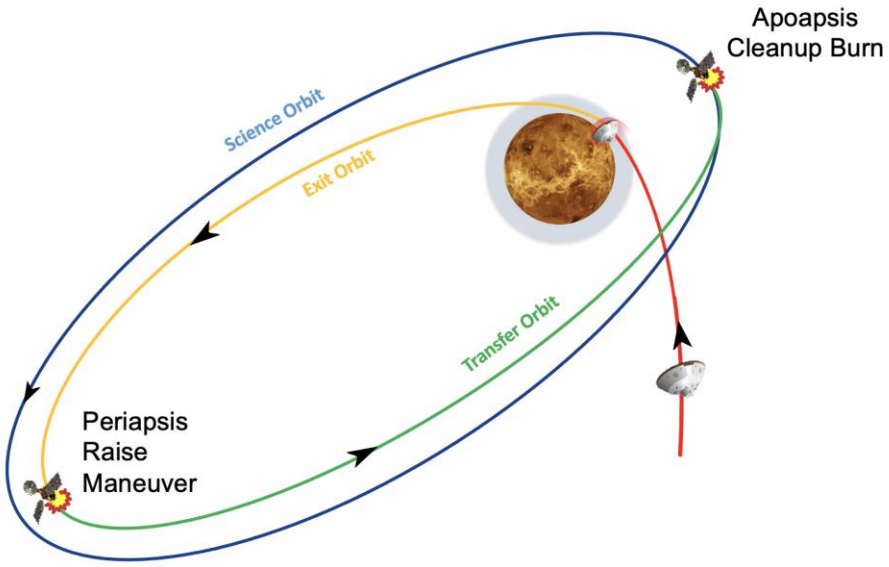

Fig. 1 Aerocapture concept of operations

Aerocapture is a similar method to aerobraking in that it utilizes atmospheric drag to decelerate the vehicle, but rather than making multiple passes, aerocapture inserts the vehicle into its captured orbit in a single pass by diving deeper into the atmosphere from an inbound hyperbolic orbit, as illustrated in Fig. 1. There are at least two propulsive maneuvers performed post-atmospheric-exit to attain the final orbit, but the majority of the deceleration occurs within the atmospheric pass, thus leading to low propellant usage compared to fully-propulsive orbit insertion. Compared to aerobraking, aerocapture is faster and can use substantially less propellant [1]. However, to date, aerocapture has not been demonstrated in-flight.

Venus is a prime candidate for demonstrating aerocapture due to its dense atmosphere. Additionally, compared to Mars, Venus is not as thoroughly explored, making it a good candidate for scientific exploration, consistently appearing as a candidate in NASA's Discovery Program. Recently, NASA selected two missions to go to Venus, including DAVINCI which will deliver the first probe to Venus in 40 years [2]. Leveraging on the renewed interest in Venus using piggy-back missions could provide increased science insight. Due to the slow rotation rate of the planet (one day on Venus spans approximately 116 Earth days [3]), exploring Venus from both the day and night side would add insight about this unique Earth neighbor. Small spacecraft on the order of a few hundred kilograms, often referred to as smallsats, offer a low-cost opportunity to explore the planet. Due to their constricted volume and low cost, attaining orbit insertion using fully-propulsive means or aerobraking adds unnecessary complexity. Thus, smallsats are ideally suited to perform aerocapture.

This paper focuses on the initial performance assessment of a Venus smallsat aerocapture mission using two separate flight dynamics simulation environments: the Program to Optimize Spacecraft Trajectories II (POST2) and Genesis. The same vehicle, mission, and planet parameters are modeled in both simulations, though differences in guidance algorithms and implementations are identified and noted. Vehicle performance between the two simulation environments in both nominal and statistically dispersed senses are compared. The performance comparison is also intended to provide an initial level of independent verification and validation (IV&V) between a flight-validated, industry-standard simulation tool (POST2) and a more recent simulation tool developed with support from the NASA Engineering Safety Center (NESC) that takes advantage of more modern programming standards and environments (Genesis).

II. Modeling & Simulation

This paper focuses on performance analysis of a spacecraft as it executes an aerocapture maneuver at Venus. Performance trades are conducted in multiple integrated simulation environments with different guidance and control algorithms to explore the design space of Venus smallsat aerocapture.

A. Vehicle and Mission Design

The vehicle used in this analysis is a notional smallsat that is deployed from a larger vehicle, such as a Venus atmospheric entry probe. A blunt body capsule configuration with a 60° sphere-cone heat shield is selected to balance steering capability and heat load. Vehicle and guidance and control (G&C) parameters are listed in Table 1. Planet and environment parameters are listed in Table 2. Initial conditions are listed in Table 3.

Table 1. Vehicle and G&C parameters.

Parameter	Value
Configuration	60° sphere-cone rigid capsule
Diameter	1 m
Mass	150 kg
Nose Radius	25% of diameter
Aerodynamics	Genesis aerodatabase [4]
Aerothermal Model	Sutton-Graves
Aerothermal Constant	0.00019
Angle of Attack Maximum Angular Rate / Acceleration	5.0°/s, 5.0°/s^2
Angle of Sideslip Maximum Angular Rate / Acceleration	5.0°/s, 5.0°/s^2
Angle of Bank Maximum Angular Rate / Acceleration	15.0°/s, 5.0°/s^2
Trim Angle of Attack (Bank Control)	-10°
Target Altitude of Apoapsis	500 km

Table 2. Planet and environment parameters.

Parameter	Value
Planet	Venus
Equatorial Radius [3]	6051.8 km
Polar Radius [3]	6051.8 km
Standard Gravitation Parameter [3]	324860 km^3/s^2
J2 [3]	4.46E-06
Rotation Period [3]	-5832.6 hours
Entry Interface Altitude	150 km
Atmosphere	VenusGRAM 2005C

Table 3. Initial conditions.

Parameter	Value
Velocity	11 km/s
Azimuth	-90°
Flight path angle	-5°
Altitude	150 km
Latitude	0
Longitude	0
Julian date	2455504.0

B. Guidance Algorithms

Two guidance algorithms will be used to compare aerocapture performance under varying G&C architectures: a generalized numerical predictor-corrector guidance (NPCG) and the Fully-Numeric Predictor-corrector Aerocapture Guidance (FNPAG) algorithm. NPCG and FNPAG are guidance methods employed by NASA Langley Research Center and Johnson Space Center. These methods are described below.

1. Generalized Numerical Predictor-Corrector Targeting Guidance (NPCG)

NPCG is a guidance framework originally developed at NASA Langley Research Center for the Mars Surveyor Program 2001 Missions [5]. The guidance framework involves invoking a predictor function to numerically integrate the vehicle state until some termination condition followed by a corrector function to solve for any control updates required to target some desired flight conditions. Since 2016, it has been extensively modified and extended to permit

a fully generalized, flexible, and robust approach to spacecraft aerocapture and entry, descent, and landing (EDL) guidance design. NPCG is structured to provide the user with a suite of fundamental generalized flight mechanics simulation algorithms, including 3DOF equations of motion, 4th-order Runge-Kutta integrator, and a projected gradient targeting system. The user, in turn, provides the necessary vehicle, planet, and atmosphere models as appropriate. The user also provides the desired steering algorithms, which can be scripted to change across different mission phases.

2. Fully-Numeric Predictor-corrector Aerocapture Guidance (FNPAG)

FNPAG is a numeric predictor-corrector guidance originally developed for aerocapture trajectories using bank control [6, 7]. The structure of the predictor is based on the optimal aerocapture trajectory, which has a bang-bang bank angle structure. The longitudinal guidance consists of two phases. In phase 1, FNPAG commands a lift-up bank angle. The predictor uses a bank angle profile which first flies the most lift-up bank angle allowed and then switches to a user-defined, lift-down bank angle. The corrector adjusts the switching time such that the desired apoapsis is achieved. When the switching time is reached, the guidance moves to phase 2. In phase 2, the predictor uses a constant bank angle profile, and the corrector solves for the constant bank angle such that the desired apoapsis is achieved. The lateral channel commands a user-specified number of bank reversals to geometrically reduce the predicted final wedge angle.

A variation of FNPAG was developed for Direct Force Control (DFC) [8]. The longitudinal channel has the same two-phase structure as the bank angle version. Optimal control theory does not reveal the optimal angle of attack command for aerocapture, but investigations with direct methods have shown that the optimal structure is very close to a lift-up, lift-down bang-bang solution [9]. The lateral channel uses a PD controller to drive the predicted final wedge angle to the desired value.

C. Steering Algorithms

Two classes of steering systems will be explored in this work. The first is the more traditional bank angle modulation (BAM), in which in the vehicle bank angle is modulated to control the lift vector. The second is DFC, in which the vehicle angle of attack is modulated to control the lift magnitude. A third control mechanism, drag modulation (DM), in which the vehicle undergoes a single-event configuration change to change the total drag force on the vehicle [10], is not considered in this analysis. Both DFC and BAM methods have unique advantages in EDL design that would feed forward into aerocapture trades and analyses.

1. Direct Force Control (DFC)

DFC is a steering method in which the angles of attack and sideslip are modulated to directly manage targeting errors. DFC is most effective when the steering channels are essentially uncorrelated, such as in the case of an axisymmetric blunt body with low to no dihedral. In this case, commanded sideslip angles do not induce vehicle roll. Additionally, if any actuated aerodynamic control surfaces such as flaps exist on the vehicle, the commanded aerodynamic angles may be achieved without propulsive burns from a reaction control system (RCS) [11]. With DFC, roll or bank control is commanded to be zero and is typically achieved with RCS.

DFC has been shown to be effective in simulated human Mars EDL scenarios with blunt bodies [12]. Fig. 2 shows how in this case, the vehicle angle of attack can be modulated to directly manage downrange errors, and vehicle sideslip angle can be modulated to directly manage crossrange errors. This same method can be applied to aerocapture, where angle of attack maps to apoapsis altitude at exit error, and sideslip angle maps to wedge angle error. DFC is intended to provide the vehicle with a level of control authority with a lower lift-to-drag ratio (L/D) that is comparable to an entry system that flies with a higher L/D and uses BAM.

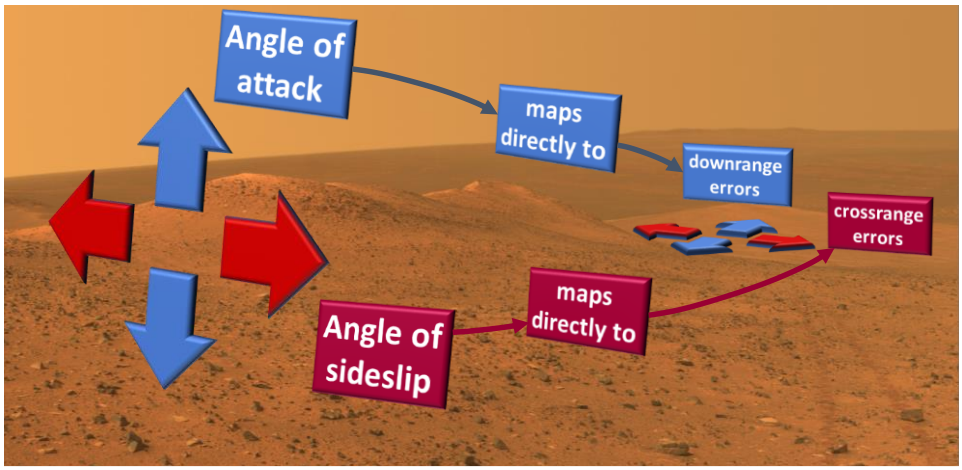

Fig. 2 Example of DFC applied to EDL [13]

2. Bank Angle Modulation (BAM)

BAM is a steering method in which the bank angle of the entry body is rotated to distribute the lift force in the side force and lift force directions, allowing the vehicle to conduct energy management while targeting desired exit conditions. This generation of lift occurs due to a designed offset center-of-gravity, allowing the vehicle to trim at a given angle of attack (and sideslip), producing lift. Fig. 3 shows how the bank angle is modulated to rotate the lift vector of an EDL vehicle to attain controllability in different directions. BAM has been used extensively at Earth, by the Gemini, Apollo [14], Space Shuttle, and Orion [15] entry systems. It has also been demonstrated at Mars as part of the Mars Science Laboratory [16] and Mars 2020 missions during the atmospheric entry phase, during which parachute deploy conditions were targeted. For BAM, apoapsis at exit and wedge angle error are managed simultaneously using bank angle. BAM allows for the vehicle to take advantage of the natural stability of the vehicle, trim angle of attack, and sideslip angle. RCS placed on the vehicle backshell is typically used for BAM, allowing control effectors to be out of the reentry heating flow.

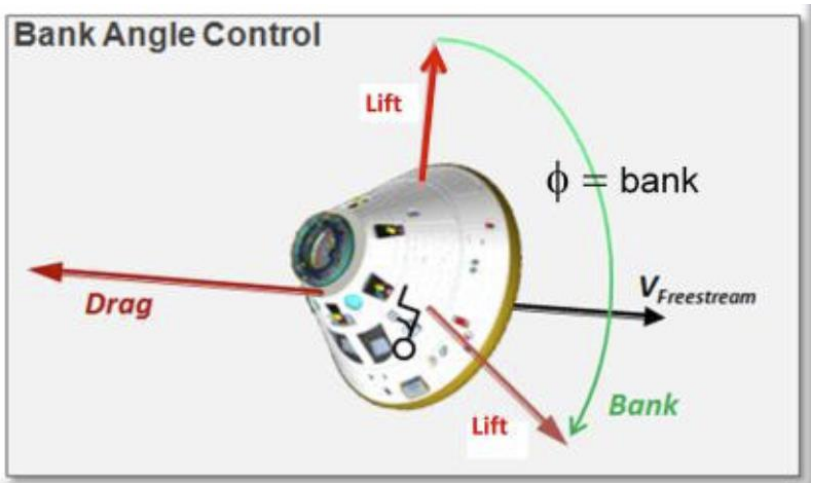

Fig. 3 Example of bank angle modulation for EDL [17]

D. Simulation Environments

Two NASA flight mechanics simulation tools are used to assess performance. The use of both simulations is part of a larger effort to help demonstrate how multiple NASA simulation tools can be quickly applied to flight mechanics problems and corroborate results. Moreover, the two simulations provide opportunities for independent verification and validation (IV&V) of the tools.

1. Program to Optimize Simulated Trajectories II (POST2)

POST2 is a flight-validated C-based simulation tool that is a rigid-body, multi-vehicle flight dynamics simulation that can provide 3-, 6-, and multi-degree-of-freedom (DOF) modeling of spacecraft both in-space and in-atmosphere [18, 19]. Based on the original POST code written to support the NASA Space Transportation System (STS) in the 1970s, the current POST2 code has been heavily updated and modularized to support multiple flight programs such as all NASA Mars atmospheric EDL systems in the past two decades [20, 21, 22, 23, 24, 25], and more recently, the NASA Space Launch System (SLS) [26], the NASA Commercial Crew Program (CCP), and the NASA Human Landing System (HLS) [27]. It has also been used to assess closed-loop guidance, navigation, and control (GN&C) performance of human-scale Mars NASA landing systems [12, 28].

2. Genesis

The second tool, Genesis, is a new flight mechanics simulation and is the successor to the Flight Analysis and Simulation Tool (FAST). Genesis is a generic, multi-vehicle, variable-degree-of-freedom flight mechanics simulation for trajectory design [29]. It enables rapid mission design and is capable of modeling ascent, aerocapture, entry, descent, and landing trajectories around a single planetary body. It is designed to be flexible, supporting low- to high-fidelity models, and easily reconfigured for new vehicles. Genesis provides generic models for atmospheric properties, winds, aerodynamics, and propulsion. It can easily be extended with new environment, vehicle, or flight software models. Genesis can be used for a wide variety of analyses, ranging from optimizing a single trajectory to running a large Monte Carlo analysis in a High-Performance Computing (HPC) environment. It consolidates and replaces a suite of NASA legacy flight mechanics simulations. It is implemented in the Julia programming language [30].

III. Results

The vehicle and trajectory described above were simulated in both POST2 and Genesis. Comma separated value (CSV) ASCII files were used to store initial states, vehicle parameters, and guidance targets. These CSV files were then directly ingested by both tools to minimize differences in inputs. Since POST2 and Genesis have different optimization routines and different implementations of the DFC and BAM steering algorithms, some differences were observed in the results and are discussed below.

A. Nominal Guided Trajectories

Time history comparisons of relevant parameters from the closed-loop guidance nominal trajectories are presented first. Fig. 4 and Fig. 5 show the nominal geodetic altitude and planet-relative velocities, respectively. Immediately it can be seen that while the Genesis DFC and BAM (written as "Bank" in the legend) are similar, the POST2 DFC trajectory is both shorter in terms of time of flight and dives deeper into the atmosphere (lower geodetic altitude). As will be shown in the following section discussion Monte Carlo performance, these differences stem from the POST2 nominal trajectory arriving at a slightly different entry flight path angle.

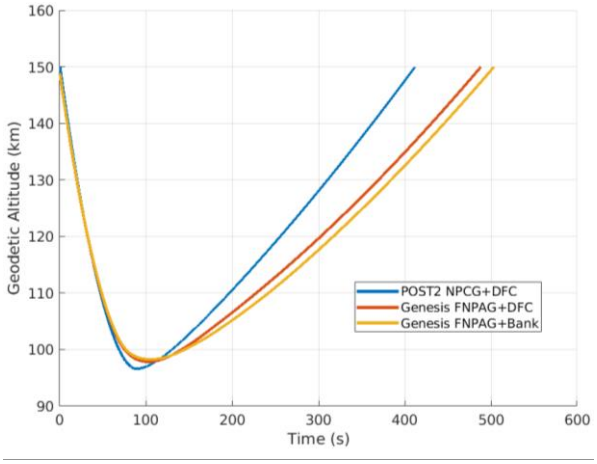

Fig. 4 Nominal geodetic altitude time history

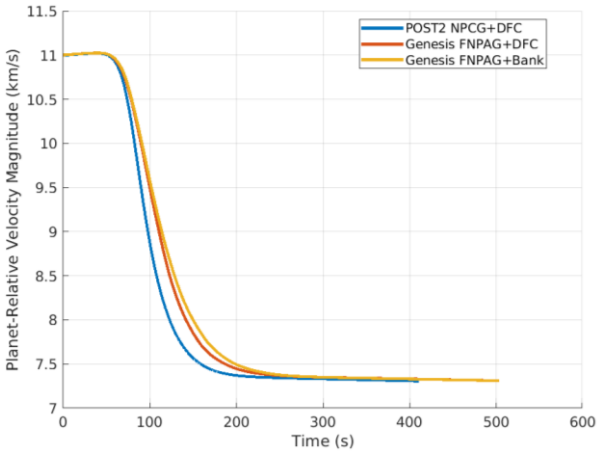

Fig. 5 Nominal planet-relative velocity

Fig. 6 and Fig. 7 show the nominal angles of attack and sideslip, respectively. Recall that with DFC, angle of attack is used to manage altitude of apoapsis error. It can be seen that the POST2 DFC angle of attack commands jumps to

approximately -9° before returning to zero. In this case, the angle of attack profile is designed around a nominal zero degree profile for both the inbound and outbound legs. This type of approach maximizes the angle of attack margin available to account for dispersions. In the Genesis/FNPAG DFC implementation, a bang-bang approach is used such that the vehicle enters at full lift-up and exits at full lift-down [9]. The Genesis DFC command begins at -10°, and some variation is seen between ±2° before it ends at 10°. For the BAM case, angle of attack is trimmed to -10°.

The POST2 simulation left angle of sideslip uncommanded, so the output for POST2 DFC is zero degrees. The Genesis implementation of FNPAG with DFC uses angle of sideslip to minimize out-of-plane errors. Though the difference in the nominal profile is relatively small, the following section will show how the dispersed cases reach higher sideslip angles. For the BAM case, angle of sideslip is left uncommanded at zero degrees.

Fig. 8 shows the bank angle profile. For the DFC cases, bank angle is zero degrees since control is provided by the angle of attack and sideslip channels. FNPAG determines the time of bank reversals and bank magnitude required to achieve the desired altitude of apoapsis and minimize out of plane errors.

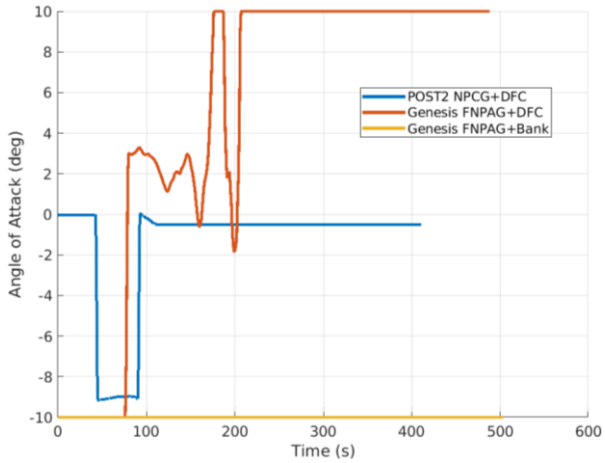

Fig. 6 Angle of attack profile

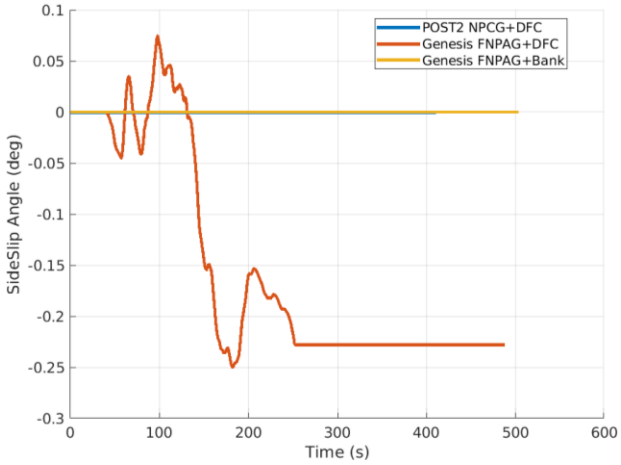

Fig. 7 Angle of sideslip profile

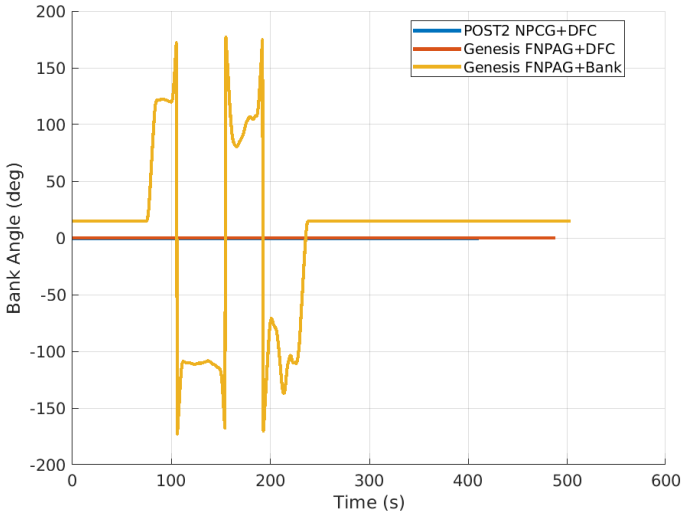

Fig. 8 Bank angle profile

Fig. 9 and Fig. 10 show the ballistic coefficient and acceleration magnitude time histories, respectively. The variation in ballistic coefficient reflects the differences in the angle of attack profiles. The acceleration magnitude shows the POST2 DFC implementation experiencing higher acceleration loads, again due to the difference in nominal entry flight path angles.

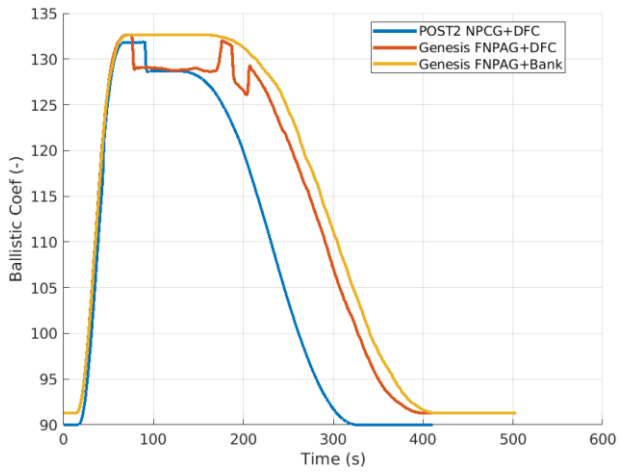

Fig. 9 Ballistic coefficient

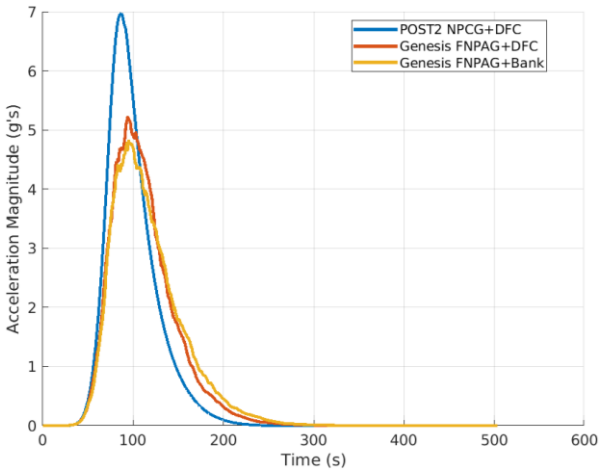

Fig. 10 Acceleration magnitude (Earth g's)

Fig. 11 and Fig. 12 show the heat rate and total heat load time histories. Given the shorter POST2 time of flight, the higher heat rate results in a lower total heat load as compared to the Genesis results. Genesis shows a slightly higher total heat load for BAM as compared to DFC. While these differences are notable, they were considered acceptable for this initial comparison effort and a Monte Carlo statistical analysis was performed as detailed in the next section.

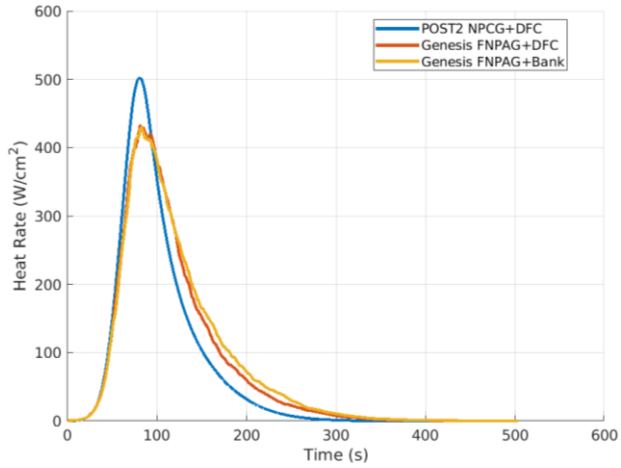

Fig. 11 Heat rate

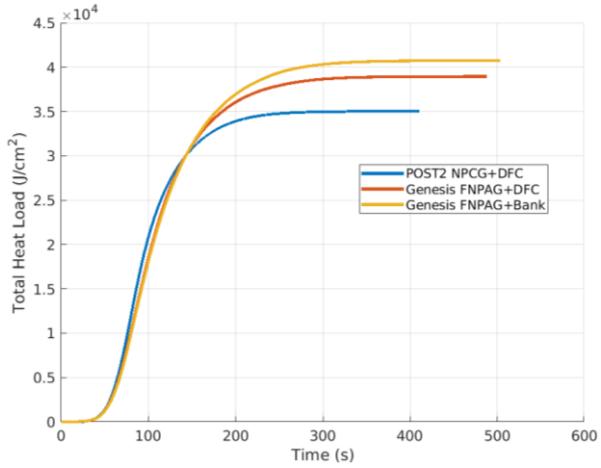

Fig. 12 Total heat load

B. Monte Carlo Analysis

Monte Carlo statistical techniques were used to assess vehicle performance. 8,000-sample (trajectory) Monte Carlos were run for each of the three cases shown in the previous section. Table 4 shows the dispersions selected for this analysis. The values were obtained from current dispersions used by the DAVINCI project [2].

Table 4. Monte Carlo dispersions.

Parameter	Units	Dispersion	Distribution
Mass	kg	0.5	3σ Normal
Atmosphere	N/A	VenusGRAM 2005C	GRAM Dispersions
Velocity	km/s	0.05045	3σ Normal
Azimuth	deg	0.022001	3σ Normal
Flight path angle	deg	0.117877	3σ Normal
Latitude	deg	0.223376	3σ Normal
Longitude	deg	0.038872	3σ Normal
Number of MC Samples	N/A	8000	3σ Normal

C. Performance

The primary performance parameter for this analysis was the target altitude of apoapsis at atmospheric exit of 500 km, shown in Fig. 13. The altitude of periapsis at atmospheric exit is shown in Fig. 14. The upper right plot shows the quantile-quantile plot, which indicates how well each distribution matches Gaussian (shown as a dotted straight line). This type of plot is useful to understand how the statistics obtained from the data may be used (e.g., the standard deviation (σ) value may be less useful if the distribution is not approximately Gaussian). In general, performance across simulation environments is comparable, though differences exist and are expected per the results shown in the nominal trajectories in the previous section. The Genesis implementation of DFC shows slightly better overall targeting performance than that of the POST2 implementation of DFC, with a smaller 3σ value and slightly better performance in the tails, the latter of which is indicated by the high and low percentiles and quantile-quantile plots. The Genesis implementation of BAM shows comparatively poorer performance, though in all three cases, better performance may likely be attained with more G&C tuning.

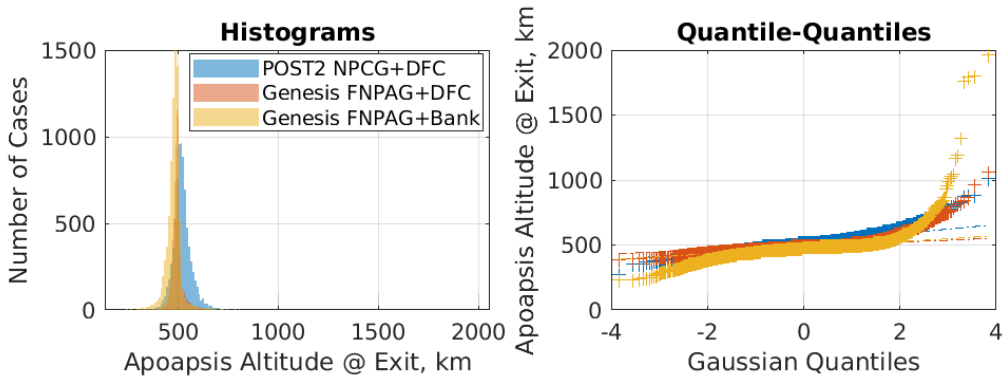

	POST2 NPCG+DFC	Genesis FNPAG+DFC	Genesis FNPAG+Bank
Mean	520.89	496.6	478.94
3-sigma	142.89	104.77	165.63
1.00 %-tile	416.57	435.35	356.02
99.00 %-tile	674.83	637.14	635.64
Max Value	1012.3	1062	1960.6
Min Value	274.21	389.4	228.43

Fig. 13 Altitude of apoapsis at atmospheric exit

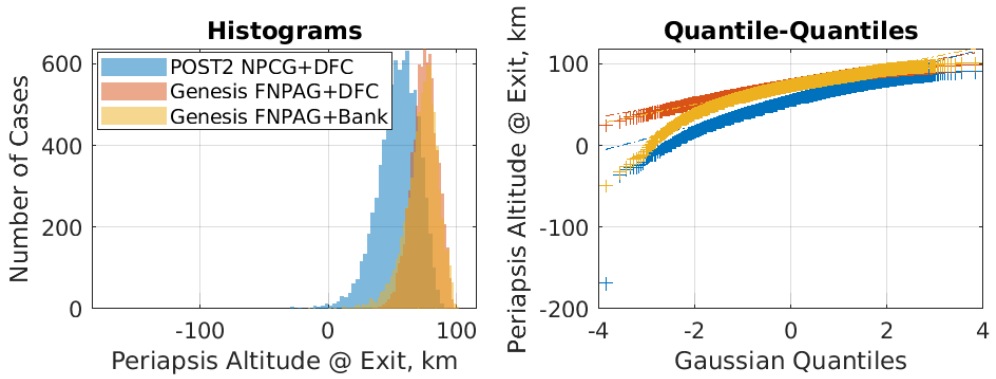

	POST2 NPCG+DFC	Genesis FNPAG+DFC	Genesis FNPAG+Bank
Mean	54.28	74.6	72.44
3-sigma	48.69	30.41	40.96
1.00 %-tile	7.31	48.4	28.61
99.00 %-tile	83.17	94.35	96.08
Max Value	91.03	98.87	101.01
Min Value	-168.21	25.3	-49.02

Fig. 14 Altitude of periapsis at atmospheric exit

Fig. 15 shows the ΔV required to insert the vehicle from its orbit at atmospheric exit, to the final 500 km by 500 km circular science orbit. This is computed assuming a Hohmann transfer orbit with two burns required to raise periapsis and adjust apoapsis. Mean values are similar between all three cases, and the NPCG implementation of DFC requires slightly more propellant than the FNPAG implementation in a 99%-tile sense. The spread for the BAM case is noticeably higher. Overall, given the assumptions and implementations in this study, DFC offers better performance than BAM.

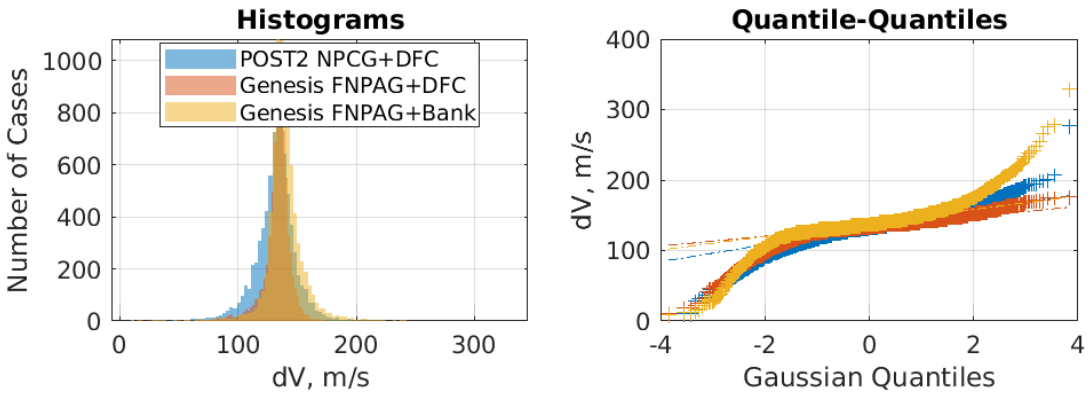

	POST2 NPCG+DFC	Genesis FNPAG+DFC	Genesis FNPAG+Bank
Mean	131.64	132.87	139.41
3-sigma	51.42	38.08	50.22
1.00 %-tile	76.28	83.93	86.92
99.00 %-tile	172.34	157.08	190.85
Max Value	277	176.49	328.8
Min Value	9.68	10.49	9.75

Fig. 15 Required clean-up ΔV

Fig. 16 shows the initial mass distribution to aid in identifying sources of difference between the simulation environments. While agreement is overall positive, there is a noted difference in the behavior of the tails between the

POST2 and Genesis simulations, which shows that the Genesis dispersed data does not follow as closely a Gaussian distribution as POST2.

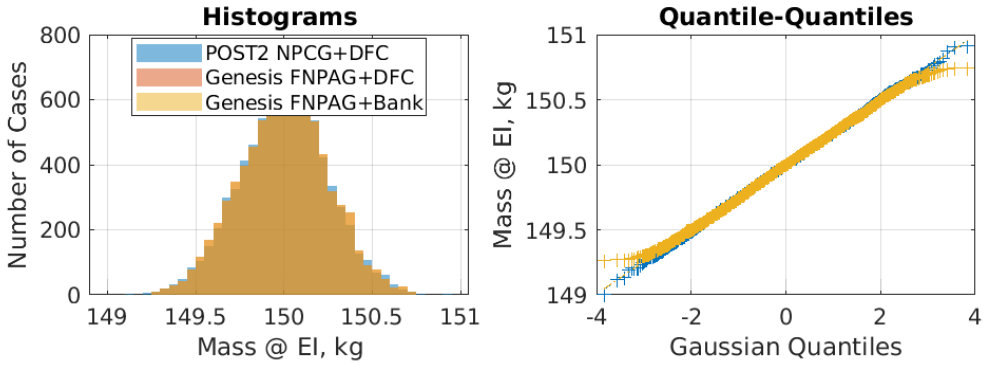

	POST2 NPCG+DFC	Genesis FNPAG+DFC	Genesis FNPAG+Bank
Mean	150	150	150
3-sigma	0.75	0.75	0.75
1.00 %-tile	149.41	149.43	149.43
99.00 %-tile	150.59	150.57	150.57
Max Value	150.91	150.75	150.75
Min Value	149	149.27	149.27

Fig. 16 Mass at entry interface

Fig. 17 shows the planet-relative flight path angle at entry interface. This parameter is one of the key optimization quantities (the other being the bang-bang switch time in the Genesis implementations of DFC and BAM), and the difference in the flight path angle chosen between the two simulations is readily apparent. This difference has implications on almost all other parameters, including peak G load and peak heat rates, that are shown and discussed elsewhere in this paper.

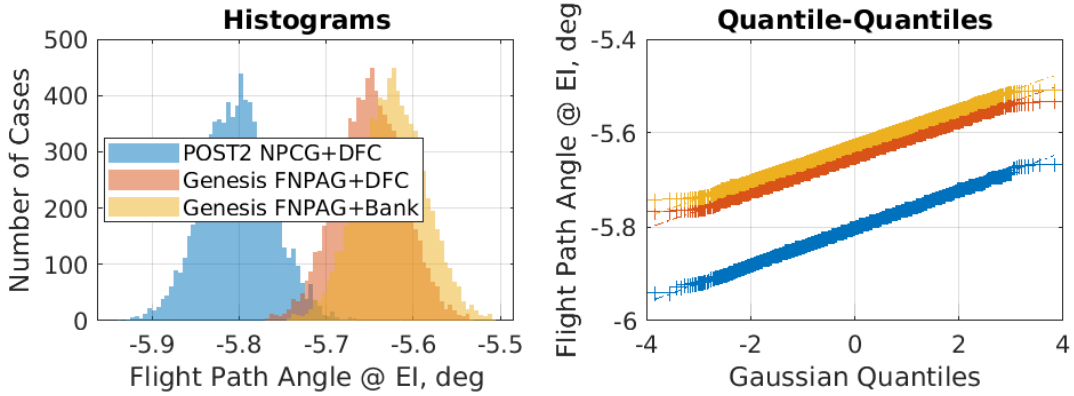

	POST2 NPCG+DFC	Genesis FNPAG+DFC	Genesis FNPAG+Bank
Mean	-5.8	-5.65	-5.62
3-sigma	0.12	0.11	0.11
1.00 %-tile	-5.89	-5.74	-5.71
99.00 %-tile	-5.71	-5.56	-5.54
Max Value	-5.67	-5.53	-5.51
Min Value	-5.94	-5.77	-5.74

Fig. 17 Planet-relative flight path angle at entry interface

Fig. 18 and Fig. 19 show the peak angle of attack and bank for each dispersed trajectory, respectively. As expected, the BAM implementation is uniformly -10°. The POST2 and Genesis DFC implementation shows almost all cases saturating at ±10°. Maximum bank angle is zero for DFC cases and ±180° for the BAM case, again due to the bang-bang optimal approach. Greater control authority is possible by increasing these command limits, and may be an area of future study.

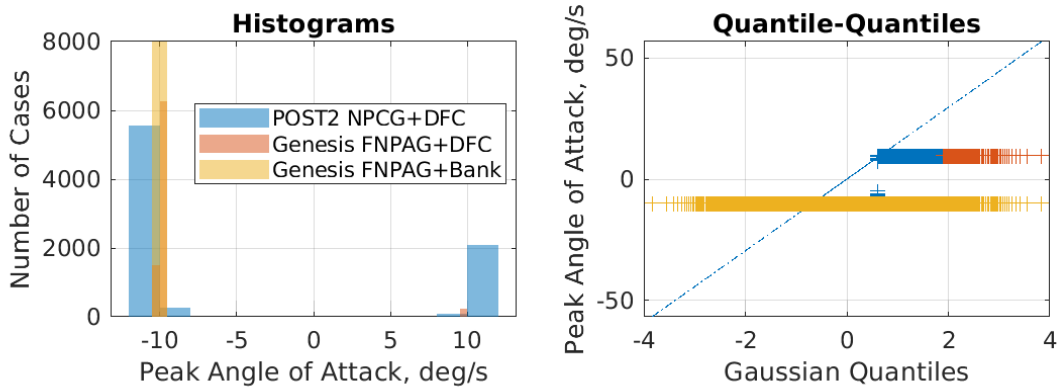

	POST2 NPCG+DFC	Genesis FNPAG+DFC	Genesis FNPAG+Bank
Mean	-4.55	-9.42	-10
3-sigma	26.64	10.07	0
1.00 %-tile	-10	-10	-10
99.00 %-tile	10	10	-10
Max Value	10	10	-10
Min Value	-10	-10	-10

Fig. 18 Peak angle of attack

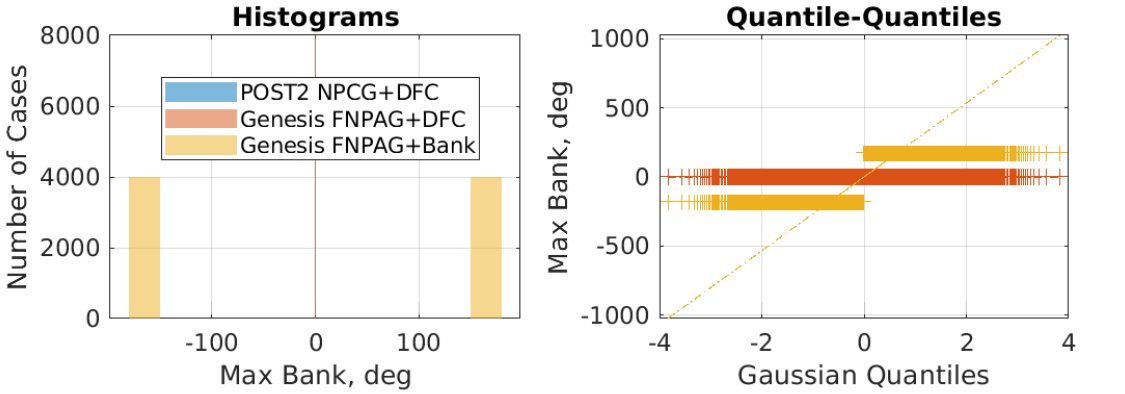

	POST2 NPCG+DFC	Genesis FNPAG+DFC	Genesis FNPAG+Bank
Mean	0	0	0.05
3-sigma	0	0	539.62
1.00 %-tile	0	0	-180
99.00 %-tile	0	0	180
Max Value	0	0	180
Min Value	0	0	-180

Fig. 19 Maximum bank angle

Fig. 20 shows the peak sensed acceleration. All values are under 10 Earth g's, which is well under typical robotic/autonomous science missions.

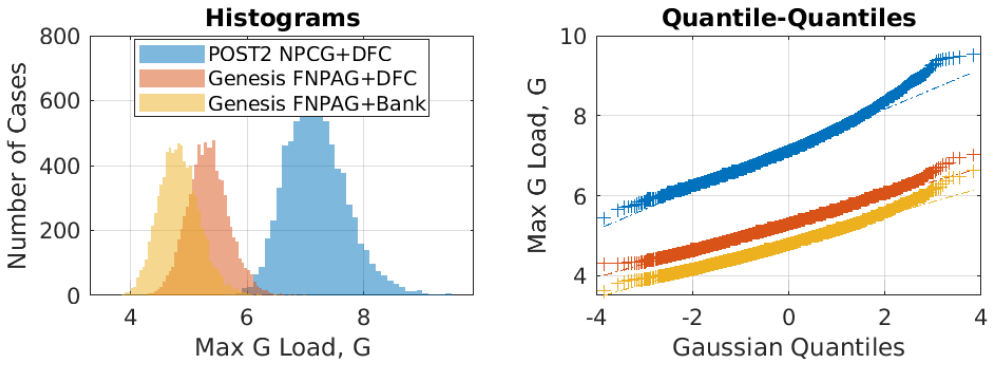

	POST2 NPCG+DFC	Genesis FNPAG+DFC	Genesis FNPAG+Bank
Mean	7.18	5.33	4.84
3-sigma	1.57	1.06	1.06
1.00 %-tile	6.13	4.57	4.1
99.00 %-tile	8.63	6.23	5.78
Max Value	9.53	7.04	6.65
Min Value	5.46	4.31	3.62

Fig. 20 Maximum sensed acceleration

Fig. 21 and Fig. 22 show the maximum heat rate and total heat load performance, respectively. Results here align with the nominal time histories.

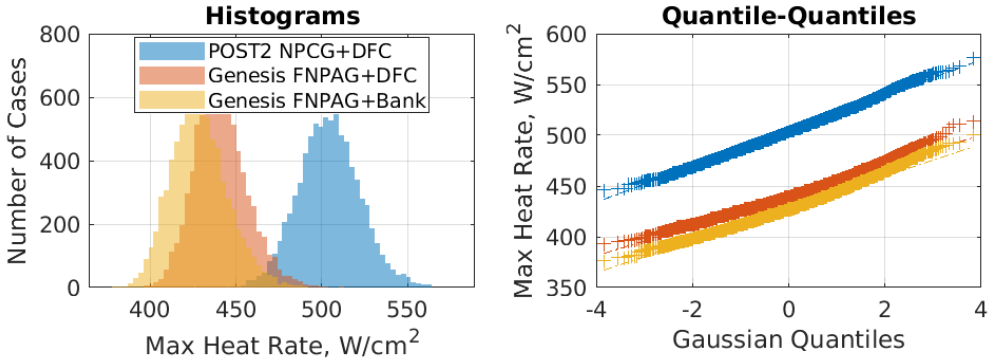

	POST2 NPCG+DFC	Genesis FNPAG+DFC	Genesis FNPAG+Bank
Mean	504.32	441.16	428.57
3-sigma	53.66	46.34	49.13
1.00 %-tile	463.86	409.31	395.27
99.00 %-tile	549.29	482.71	471.61
Max Value	576.8	514.34	500.57
Min Value	446.67	392.77	376.53

Fig. 21 Maximum heat rate performance

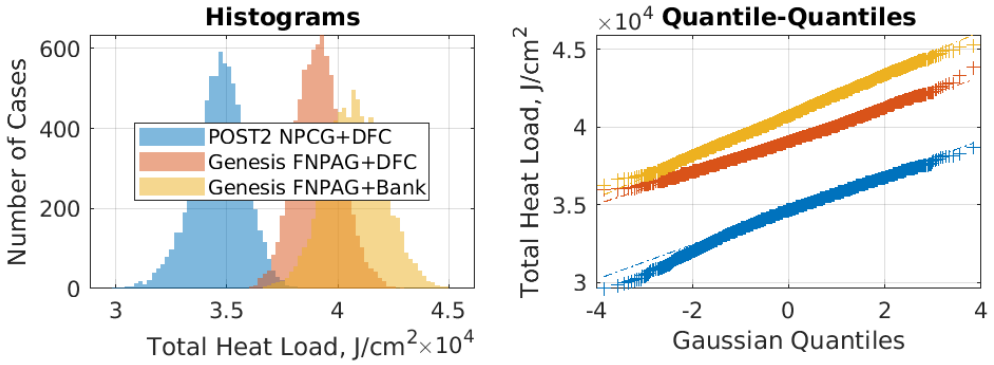

	POST2 NPCG+DFC	Genesis FNPAG+DFC	Genesis FNPAG+Bank
Mean	34627	39125	40772
3-sigma	3519	3081.1	3927.3
1.00 %-tile	31580	36812	37769
99.00 %-tile	37136	41669	43810
Max Value	38668	43812	45268
Min Value	29603	35927	36264

Fig. 22 Total heat load performance

From this analysis, a set of performance parameters listed in Table 5 was assembled as a suggestion for future aerocapture-based simulation comparisons. Initial states and conditions may be used to ensure consistency between simulation environments.

Table 5 Suggested aerocapture performance parameters for simulation comparisons

Parameter	Units
Initial mass	kg
Initial states (e.g., orbital elements)	various
Entry flight path angle	degrees
Peak dynamic pressure	Pascals
Peak heat rate	W/cm^2
Peak G load	Earth G's
Total heat load	J/cm^2
Time of atmospheric flight	seconds
Minimum Mach number	N/A
Minimum geodetic altitude	kilometers
Altitude of periapsis at atmospheric exit	kilometers
Altitude of apoapsis at atmospheric exit	kilometers
Wedge angle error at atmospheric exit	degrees
Inclination at atmospheric exit	degrees
Longitude of ascending node at atmospheric exit	degrees
Maximum angle of attack	degrees
Maximum angle of sideslip	degrees
Maximum bank angle	degrees
Cleanup dV	m/s

IV. Summary and Conclusions

The aerocapture problem at Venus was investigated within the context of a "first step" in establishing a simulation comparison process using a non-trivial flight mechanics problem with integrated closed-loop guidance algorithms. Differences in simulation environments were identified and mapped to performance differences. Overall solutions between simulations and algorithms were comparable and showed favorable performance, though additional G&C tweaking and optimization may net further performance. Additional work remains to align initial conditions and certain assumptions to improve comparisons. Future work currently scheduled includes applying the same tools to a more complex flight mechanics problem: EDL.

Acknowledgments

The authors acknowledge the support from the NASA Space Technology Mission Directorate (STMD) through the Entry Systems Modeling (ESM) project that funded the efforts detailed in this paper. Additionally, some of the guidance and control methods utilized in this paper were developed with the assistance of Rohan Deshmukh, Ping Lu, Kyle Webb, Casey Heidrich, and Alicia Cianciolo.

References

[1] Hall, J. L., Noca, M. A., and Bailey, R. W., "Cost-Benefit Analysis of the Aerocapture Mission Set," *Journal of Spacecraft and Rockets*, Vol 42, No. 2, 2005, pp 309-320, doi: 10.2514/1.4118.

[2] Dutta, S., Guecha-Ahumada, N. G, Garrison, M. B., Hughes, K. M., and Johnson, M. Z., "DAVINCI Venus Entry, Descent, and Landing Modeling and Simulation," AIAA SciTech 2023, AIAA Atmospheric Flight Mechanics Conference, National Harbor, MD.

[3] Williams, D. R., "Venus Fact Sheet," [website], URL: https://nssdc.gsfc.nasa.gov/planetary/factsheet/venusfact.html [retrieved 15 November 2022].

[4] Desai, P. N., Qualls, G. D., and Schoenenberger, M., "Trajectory Reconstruction for the Genesis Entry," Proceedings of the 3rd International Planetary Probe Workshop, Anavyssos, Greece, Jun. 2005.

[5] Lugo, R. A., et al., "Overview of a Generalized Numerical Predictor-Corrector Targeting Guidance with Application to Human-Scale Mars Entry, Descent, and Landing," AIAA 2020-0846, 2020.

[6] Lu, P., Cerimele, C. J., Tigges, M. A., and Matz, D. A., "Optimal Aerocapture Guidance," *Journal of Guidance, Control, and Dynamics*, Vol. 38, No. 4, 2015, pp 553–565. http://dx.doi.org/10.2514/1.g000713.

[7] Webb, K., Lu, P., and Dwyer-Cianciolo, A., "Aerocapture Guidance for Human Mars Missions," AIAA 2017-1900, AIAA SciTech 2017, AIAA Guidance, Navigation, and Control Conference, Grapevine, TX, 2017.

[8] Matz, D. A., and Cerimele, C. J., "Development of a Numeric Predictor-Corrector Aerocapture Guidance for Direct Force Control," AIAA 2020-0847, 2020.

[9] Geiser, J. K, and Matz, D. A., "Optimal Angle of Attack Control for Aerocapture," AIAA 2022-0608, 2022.

[10] Roelke, E., and Braun, R. D., "Discrete-Event Drag-Modulated Guidance Performance for Venus Aerocapture," *Journal of Spacecraft and Rockets*, Vol. 58, No. 1, 2021, pp 190-199, doi: 10.2514/1.A34761.

[11] Margolis, B., Okolo, W., D'Souza, S., and Johnson, B., "Pterodactyl: Guidance and Control of a Symmetric Deployable Entry Vehicle using an Aerodynamic Control System", AIAA 2021-0764, 2020 https://doi.org/10.2514/6.2021-0764.

[12] Lugo, R. A., et al., "Overview of a Generalized Numerical Predictor-Corrector Targeting Guidance with Application to Human-Scale Mars Entry, Descent, and Landing," AIAA 2020-0846, 2020.

[13] Lugo, R. A., Karlgaard, C. D., Powell, R. W., and Cianciolo, A. D., "Integrated Flush Air Data Sensing System Modeling for Planetary Entry Guidance with Direct Force Control," AIAA 2019-0663.

[14] Graves, C., and Harpold, J., "Apollo Experience Report: Mission Planning for Apollo Reentry," NASA TN-D-6725, March 1972.

[15] Putnam, Z. R., Neave, M. D., and Barton, G. H., "PredGuid Entry Guidance for Orion Return from Low Earth Orbit," IEEE Paper 2010- 1571, March 2010.

[16] Mendeck, G. F., and McGrew, L. C., "Entry Guidance Design and Postflight Performance for 2011 Mars Science Laboratory Mission," Journal of Spacecraft and Rockets, Vol. 51, No. 4, July-August 2014.

[17] Tigges, M. A, Bihari, B. D., Stephens, J-P, Vos, G. A., Bilimoria, K. D., Mueller, E. R., Law, H. G., Johnson, W., Bailey, R. E., and Jackson, B., "Orion Capsule Handling Qualities for Atmospheric Entry," AIAA 2011-6264, AIAA Guidance, Navigation, and Control Conference, Portland, OR.

[18] Lugo, R. A., Shidner, J.D, Powell, R.W., Marsh, S.M., Hoffman, J.A., Litton, D.K., and Schmitt, T.L., "Launch Vehicle Ascent Trajectory Simulation Using the Program to Optimize Simulated Trajectories II (POST2)," AAS 17-274, AAS Space Flight Mechanics Meeting, San Antonio, TX.

[19] Williams, R. A., Lugo, R. A., Marsh, S. M, Hoffman, J. A., Shidner, J. D., and Aguirre, J. T., "Enabling Thread Safety and Parallelism in the Program to Optimize Simulated Trajectories II," AIAA SciTech 2023, National Harbor, MD.

[20] Braun, R. D., Powell, R. W., Engelund, W. C., Gnoffo, P. A., Weilmuenster, K. J., and Mitcheltree, R. A., "Mars Pathfinder Six-Degree-of-Freedom Entry Analysis," *Journal of Spacecraft and Rockets*, Vol. 32, No. 6, 1995, pp. 993–1000, doi:10.2514/3.26720.

[21] Desai, P. N., Schoenenberger, M., and Cheatwood, F. M., "Mars Exploration Rover Six-Degree-of-Freedom Entry Trajectory Analysis," *Journal of Spacecraft and Rockets*, Vol. 43, No. 5, 2006, pp. 1019–1025, doi:10.2514/1.6008

[22] Desai, P. N., Prince, J. L., Queen, E. M., Schoenenberger, M., Cruz, J. R., and Grover, M. R., "Entry, Descent, and Landing Performance of the Mars Phoenix Lander," *Journal of Spacecraft and Rockets*, Vol. 48, No. 5, 2011, pp. 798–808, doi:10.2514/1.48239

[23] Striepe, S. A. et al, "Mars Science Laboratory Simulations for Entry, Descent, and Landing", *Journal of Spacecraft and Rockets*, Vol. 43, No. 2, 2006, pp. 311-323, doi: 10.2514/1.19649.

[24] Maddock, R. W., et al., "InSight Entry, Descent, and Landing Postflight Performance Assessment", *Journal of Spacecraft and Rockets*, Vol. 58, No. 5, 2021 pp. 1530-1537.
[25] Way, D. W. et al., "Assessment of the Mars 2020 Entry, Descent, and Landing Simulation", AIAA Atmospheric Flight Mechanics Conference 2022, AIAA 2022-0421, 2022.
[26] Albertson, C. W. et al., "End-To-End Simulation of Launch Vehicle Trajectories Including Stage Separation Dynamics", AIAA 2012-4863. AIAA Atmospheric Flight Mechanics Conference. August 2012
[27] Lugo, R. A., et al., "Precision Landing Performance of a Human-Scale Lunar Lander Using a Generalized Simulation Framework," AIAA 2022-0609, 2022.
[28] Lugo, R. A., et al., "Integrated Precision Landing Performance and Technology Assessments of a Human-Scale Mars Lander Using a Generalized Simulation Framework," AIAA 2022-0607, 2022.
[29] Murri, D. et al., "Improvements to the Flight Analysis and Simulation Tool (FAST) and Initial Development of the Genesis Flight Mechanics Simulation for Ascent, Aerocapture, Entry, Descent, and Landing (A2EDL) Trajectory Design," NASA TM-20210014622, 2021.
[30] "The Julia Programming Language," [website], URL: https://julialang.org [retrieved 15 November 2022].